

Higher-order-mode assisted silicon-on-insulator 90 degree polarization rotator

Yang Yue^{1*}, Lin Zhang¹, Muping Song², Raymond G. Beausoleil³, and Alan E. Willner¹

¹Department of Electrical Engineering, University of Southern California, Los Angeles, CA 90089, USA

²Department of Information and Electronic Engineering, Zhejiang University, Hangzhou, Zhejiang, 310027, China

³HP Laboratories, Palo Alto, CA 94304, USA

*yyue@usc.edu

Abstract: We propose and analyze a 90° polarization rotator based on wave coupling through an intermediate, multimode, axially uniform waveguide. The coupling efficiency of the *x*- and *y*-polarized fundamental modes between the horizontal and vertical rectangular waveguides is remarkably enhanced with the help of the TE₀₁ mode in the multimode waveguide. The polarization rotator has a very short (21-μm) conversion length with a 17.22 dB extinction ratio. It also exhibits a 68-nm bandwidth for polarization conversion efficiency above 90%.

©2009 Optical Society of America

OCIS codes: (130.2790) Guided waves; (130.3120) Integrated optical devices; (130.5440) Polarization-sensitive devices; (230.3990) Micro-optical devices; (230.7370) Waveguides.

References and links

1. C. Vinegoni, M. Karlsson, M. Petersson, and H. Sunnerud, "The statistics of polarization-dependent loss in a recirculating loop," *J. Lightwave Technol.* **22**(4), 968–976 (2004).
2. X. B. Yu, H. Y. Zhang, and X. P. Zheng, "High carrier suppression double sideband modulation using polarization state rotation filter and optical external modulator," *Opt. Commun.* **267**(1), 83–87 (2006).
3. C. E. Socolich, and M. N. Islam, "Fiber polarization-rotation switch based on modulation instability," *Opt. Lett.* **14**(12), 645–647 (1989).
4. T. Barwicz, M. R. Watts, M. A. Popovic, P. T. Rakich, L. Socci, F. X. Kartner, E. P. Ippen, and H. I. Smith, "Polarization-transparent microphotonic devices in the strong confinement limit," *Nat. Photonics* **1**(1), 57–60 (2007).
5. Y. Ohmachi, and J. Noda, "LiNbO₃ TE-TM mode converter using collinear acoustooptic interaction," *IEEE J. Quantum Electron.* **13**(2), 43–46 (1977).
6. R. C. Alferness, and L. L. Buhl, "Waveguide electrooptic polarization transformer," *Appl. Phys. Lett.* **38**(9), 655–657 (1981).
7. N.-N. Feng, R. Sun, J. Michel, and L. C. Kimerling, "Low-loss compact-size slotted waveguide polarization rotator and transformer," *Opt. Lett.* **32**(15), 2131–2133 (2007).
8. A. D. Bristow, V. N. Astratov, R. Shimada, I. S. Culshaw, M. S. Skolnick, D. M. Whittaker, A. Tahraoui, and T. F. Krauss, "Polarization conversion in the reflectivity properties of photonic crystal waveguides," *IEEE J. Quantum Electron.* **38**(7), 880–884 (2002).
9. T. Mangeat, L. Escoubas, F. Flory, L. Roussel, M. De Micheli, and P. Coudray, "Integrated polarization rotator made of periodic asymmetric buried Ta₂O₅ / silica sol-gel waveguides," *Opt. Express* **15**(19), 12436–12442 (2007), <http://www.opticsinfobase.org/oe/abstract.cfm?URI=oe-15-19-12436>.
10. H. Fukuda, K. Yamada, T. Tsuchizawa, T. Watanabe, H. Shinojima, and S. Itabashi, "Polarization rotator based on silicon wire waveguides," *Opt. Express* **16**(4), 2628–2635 (2008), <http://www.opticsinfobase.org/oe/abstract.cfm?URI=oe-16-4-2628>.
11. Z. Wang, and D. Dai, "Ultrasmall Si-nanowire-based polarization rotator," *J. Opt. Soc. Am. B* **25**(5), 747–753 (2008).
12. H. Deng, D. O. Yevick, C. Brooks, and P. E. Jessop, "Design Rules for Slanted-Angle Polarization Rotators," *J. Lightwave Technol.* **23**(1), 432–445 (2005).
13. Y. Yue, L. Zhang, M. Song, R. G. Beausoleil, and A. E. Willner, "On-Chip 90 Degree Polarization Rotator Using Wave Coupling through an Intermediate, Multimode, Uniform Waveguide," in *Optical Fiber Communication Conference*, OSA Technical Digest (CD) (Optical Society of America, 2009), paper OTuL6.
14. J. P. Donnelly, H. A. Haus, and N. Whitaker, "Symmetric three-guide optical coupler with nonidentical center and outside guides," *IEEE J. Quantum Electron.* **23**(4), 401–406 (1987).

1. Introduction

Polarization of an optical wave is at the heart of different data degrading effects, such as polarization-dependent-loss/gain and polarization-mode-dispersion [1], and a key enabler of

various signal processing functions, such as polarization-rotation-based modulation and switching [2,3]. Therefore, the control and rotation of a signal's state-of-polarization is quite desirable, especially in future, cost-effective, and on-chip planar photonic integrated circuits.

For high index-contrast integrated waveguides, one of the main issues is their strong polarization dependence. To overcome this drawback, a polarization diversity system consisting of polarization splitters and rotators has been proposed [4]. A polarization diversity system enables polarization-insensitivity to input light with arbitrary polarization, but may require a polarization rotator as one of the core devices.

The simple act of on-chip rotation of the polarization by 90° is not trivial. To realize polarization rotation, methods such as acousto-optic [5] or electro-optical [6] effects have been used. Passive polarization rotators have also been studied extensively. Reported techniques that require precise fabrication of longitudinally varying structures include using waveguide tapers [7], photonic crystal patterns [8], periodic asymmetric waveguides [9], and an off-axis double-core structure [10,11]. Slanted-sidewall waveguides were also used to realize polarization rotation [12]. A polarization rotator with a uniform and vertical sidewall structure over propagation direction is highly desired to reduce the fabrication complexity [13].

In this paper, we propose and simulate an on-chip 90° polarization rotator using wave coupling through an intermediate, multimode, uniform waveguide (WG). The coupling efficiency of the x - and y -polarized fundamental modes between the horizontal and vertical rectangular waveguides is remarkably enhanced by their proximity to the TE_{01} mode in the multimode waveguide. This newly designed polarization rotator has a very short polarization conversion length ($\sim 21\mu\text{m}$). We note that the extinction ratio is above 17dB. It also exhibits a 68 nm bandwidth for polarization conversion efficiency (PCE) above 90%. Also, the proposed design is not limited to silicon-on-insulator (SOI) waveguides but could also be used in other waveguides, such as III-V waveguides and photonic crystal fibers, to realize polarization rotation.

2. Concept and principle of operation

To achieve efficient energy transfer and mode coupling among waveguides, there are two important rules. One is that the effective refractive indices of the modes should match each other, and the other is that the directions of the electric fields of the modes in the coupling area should not be orthogonal to each other. The coupling coefficient is highly related with these two conditions. Figure 1(a) and 1(b) show the coupling efficiency of coupled waveguides with the 90° rotated mirror structure. The simulation results indicate that the electric fields of the refractive index matched waveguides, as illustrated in Fig. 1(a), cannot couple with each other, which is attributed to the fact that their electric fields are mostly orthogonal to one another. For the structure in Fig. 1(b), the modes of the two waveguides can couple mutually and generate two supermodes, which are analogous to a symmetric mode and antisymmetric mode in regular directional couplers. Although the electric fields have parallel components within the coupling region, the coupling effect is very weak since the coupling length of these two waveguides is relatively long. We find that the coupling length of scheme (b) is around 1.2 mm for the same structural parameters as in scheme (c). We introduce WG 2 near WGs 1 and 3 so as to enhance the coupling between WGs 1 and 3 and make the polarization rotator more compact, as illustrated in Fig. 1(c). The electric field of the TE_{01} mode in WG 2 has a parallel electric field component to that of x -polarized fundamental mode in WG 1. Also, WG 2 has a parallel electric field component to that of the y -polarized fundamental mode in WG 3. Good electric field alignment produces a large coupling coefficient, which gives efficient energy transfer. As a result, the coupling length of scheme (c) is reduced to $21\mu\text{m}$, only $1/60$ of the coupling length for scheme (b).

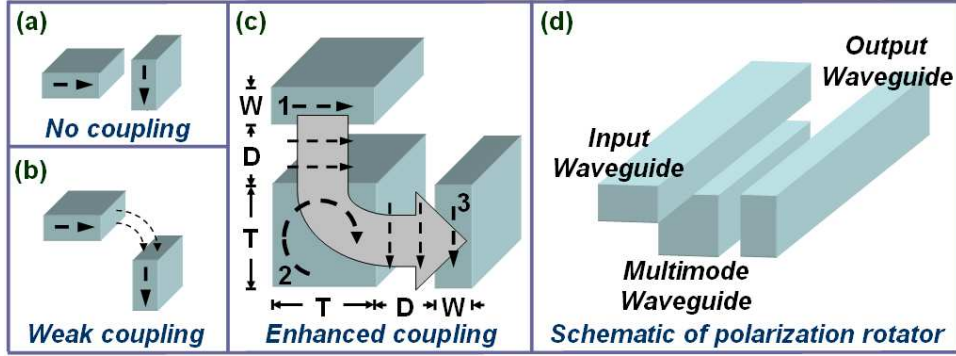


Fig. 1. Operating principle (a) No coupling case. (b) Weak coupling case. (c) Proposed 90° polarization rotator using wave coupling through an intermediate multimode waveguide. (d) Schematic of proposed 90° polarization rotator.

A full-vector finite element method (FEM) is used to analyze the mode properties, which can give an accurate solution for the field distributions. WGs 1, 2 and 3 are made of silicon and we choose silica as the cladding. We obtain the refractive indices of silicon and silica according to the Sellmeier equation in our model, taking the material dispersion into account. The refractive indices of silicon and silica at 1550 nm are 3.4764 and 1.4440, respectively. To match the effective refractive index of the TE₀₁ mode in multimode WG 2 with those of the x- and y-polarized fundamental modes in WGs 1 and 3, the parameters of W = 182 nm, D = 300 nm and T = 500 nm are chosen.

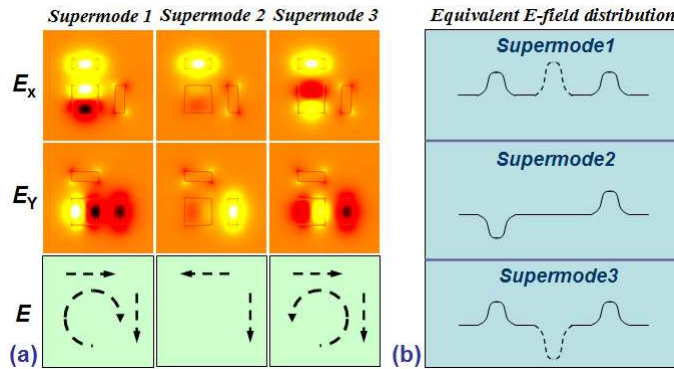


Fig. 2. (a) X-, Y- polarized electric field distributions and electric field lines of the three supermodes in the proposed waveguide structure. (b) Equivalent E-field distribution of the supermodes in three waveguides (solid line: fundamental modes, dot line: TE₀₁ mode).

There are three supermodes in this three-waveguide structure as it is similar to a three-core directional coupler [14]. Figure 2(a) shows the two orthogonal x- and y- polarized electric fields of these two symmetric and one antisymmetric modes. The figures in the bottom row also show the electric field lines within the waveguides for different supermodes. According to the relationship of electric field lines in adjacent waveguides (WG 1-2, WG 2-3), we get the equivalent E-field distribution for the three supermodes as shown in Fig. 2(b). The solid line represents the fundamental mode, while the dotted line denotes the TE₀₁ mode. If the electric field lines of the adjacent waveguides are of the same direction, then the equivalent E-field distribution will have the same polarity; otherwise, the polarity will change. Figure 3(a) shows the effective indices of the three supermodes and Fig. 3(b) illustrates the conversion lengths as a function of wavelength. The modal conversion length between WGs 1 and 3 is determined by

$$L_{c1} = \lambda / [2 \times (n_{eff1} - n_{eff2})] \quad (1)$$

while the conversion length for the TE₀₁ order mode in WG 2 is obtained from

$$L_{c2} = \lambda / [2 \times (n_{eff1} - n_{eff3})]. \quad (2)$$

Here, n_{eff1} , n_{eff2} and n_{eff3} are the effective refractive indices of the supermode 1, 2 and 3 respectively. The effective refractive indices of the supermodes are equally spaced, i.e.,

$$n_{eff1} - n_{eff3} = 2 \times (n_{eff2} - n_{eff3}) \quad (3)$$

to obtain a highly efficient power transfer between WGs 1 and 3. According to these equations, we can also find that $L_{c1} = 2L_{c2}$ is the optimized case (short conversion length and high conversion efficiency). From Fig. 3(b) we can see that 1543 nm emerges to be the optimized wavelength for the structure parameters we choose.

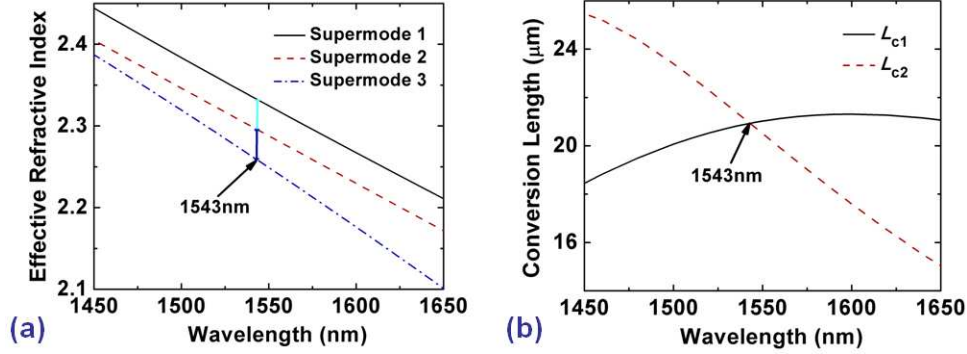


Fig. 3. (a) Effective refractive indices of the three supermodes in Fig. 2 as a function of wavelength. (b) Conversion lengths of the fundamental and TE₀₁ modes.

3. Characterization

We obtain the electric field (E) distribution and propagation constant (β) of the each supermode through FEM mode solver. In our current configuration, we can calculate E_z to be less than 10^{-3} of E_x and E_y allowing us to consider the x - and y - components of E . By substituting them into Eq. (4), we further verify the propagation characteristics of the proposed polarization rotator.

$$\vec{E}(x, y) = k_1 \vec{E}_1(x, y) e^{i\beta_1 z} + k_2 \vec{E}_2(x, y) e^{i\beta_2 z} + k_3 \vec{E}_3(x, y) e^{i\beta_3 z} \quad (4)$$

where the vector field in term of the components can be expressed as

$$\vec{E}(x, y) = E_x(x, y)\hat{x} + E_y(x, y)\hat{y}, \quad \vec{E}_i(x, y) = E_{ix}(x, y)\hat{x} + E_{iy}(x, y)\hat{y},$$

and k_i is the normalized coefficient for the linear superposition of the supermodes to generate an electric field input only in WG 1, where $i = 1, 2, 3$ for three different supermodes.

Figure 4(a) and 4(b) show the normalized power transfer of the x - and y - polarizations along the propagation distance. We note that the conversion length of the power from WG 1 to WG 3 is around 21 μm , which is twice the conversion length of the TE₀₁ mode in WG 2. This result is in good agreement with the conversion length estimated by using Eq. (1) and (2) since E_z is relatively small. From 0 μm to 10.5 μm , the energy is transferred from the x -polarized fundamental mode in WG 1 to the TE₀₁ mode in WG 2. Meanwhile, the TE₀₁ mode in WG 2 is coupled with the y -polarized fundamental mode in WG 3 and transfers the power to WG 3. In this process, the power in WG 1 decreases while the power accumulates in WG 2 and WG 3. At the end of this process (10.5 μm), the power in WG 1 is equal to the power of WG 2 along the x -polarization, and the power of WG 2 along the y -polarization is equal to the power in WG 3. From 10.5 μm to 21 μm , the powers in WGs 1 and 2 decrease simultaneously and transfer to WG 3, resulting in the power in WG 3 reaching its maximum at 21 μm . The

result illustrates that an extinction ratio of 17.22 dB can be achieved, which shows the best case of polarization conversion from WG 1 to WG 3 using the proposed structure.

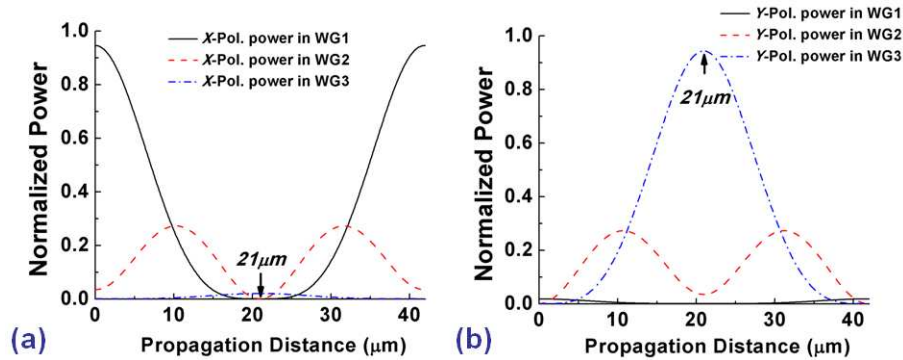


Fig. 4. (a) X-polarized normalized power exchange along the propagation distance in three waveguides. (b) Y-polarized normalized power exchange along the propagation distance in three waveguides.

PCE is a key parameter in evaluating the property of polarization rotators, which is defined as the percentage of the power transfer from the input polarized mode to the output orthogonally polarized mode. We further examine the PCE as a function of wavelength in order to evaluate the performance of the proposed polarization rotator. Figure 5 indicates that, for a PCE above 90%, the polarization rotator with the proposed parameters has a 68-nm bandwidth around 1543 nm.

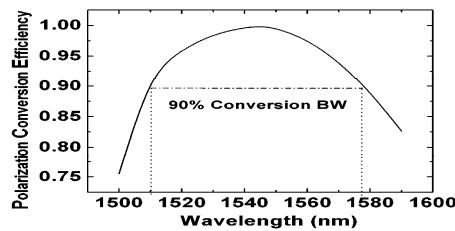


Fig. 5. PCE as a function of wavelength and >90% PCE Bandwidth.

4. Fabrication tolerance

For the submicron and high index contrast waveguides, the accuracy of fabrication is still an important factor which should be taken into account. Figure 6(a) and 6(b) show the PCE variation for different waveguide distances (D) and waveguide widths (W), while the size of multimode waveguide (T) remains the same. The solid lines correspond to the PCE for a waveguide of 21 μm length. We find that the D tolerance is around 40 nm and the W tolerance is only about 6 nm to keep the PCE above 90%. This is attributed to the fact that the variation of W significantly affects the effective refractive indices of the three supermodes compared with the variation of D . The dash-dotted line and dashed line represent the corresponding conversion lengths for the maximal PCE. In the case of imprecise D , optimizing the length of WG ($L_{c\max}$) accordingly can largely compensate for the PCE. Figure 6(a) shows that for a ± 50 nm variation, the maximal PCE can still achieve 95%, while for the case of nonideal W , even with the optimized conversion length $L_{c\max}$, the PCE can only improve a little. Here, the effect of the compensation is related to the slope of the $L_{c\max}$ curve. Also, PCE can achieve its maximum with a proper wavelength, where Eq. (3) holds.

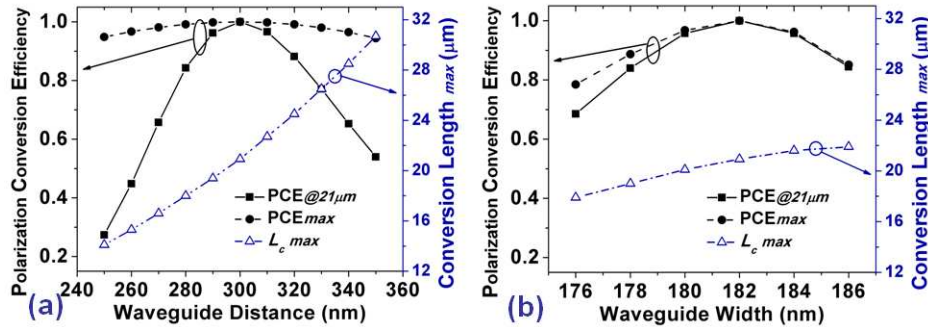


Fig. 6. (a) PCE@21 μ m, optimized PCE and its corresponding conversion length as a function of waveguide distance (D). (b) PCE@21 μ m, optimized PCE and its corresponding conversion length as a function of waveguide width (W).

The fabrication tolerance shown in Fig. 6(a) and 6(b) is based on the same D and W variation of WG 1 and 3. In reality, a different D and W variation is much more common during fabrication. Figure 7(a) and 7(b) further show the PCE for varying only one of the WG's D and W values, while keeping other parameters unchanged. For the ΔD and ΔW variations of one WG, we obtain results similar to the D and W variation of WG 1 and 3, indicating that the ΔD tolerance is much better than ΔW . From Fig. 7(a) we observe that for the optimized conversion length, a 90% PCE can be achieved for a ± 40 -nm ΔD variation. For ΔW , a ± 5 -nm change will decrease the PCE to 70%. There are several steps of depositing and etching to fabricate the proposed structure. It is important to mention that there might be some bumps in the layer between WG 1 and 2, 3 during fabrication and thus bending WG 1.

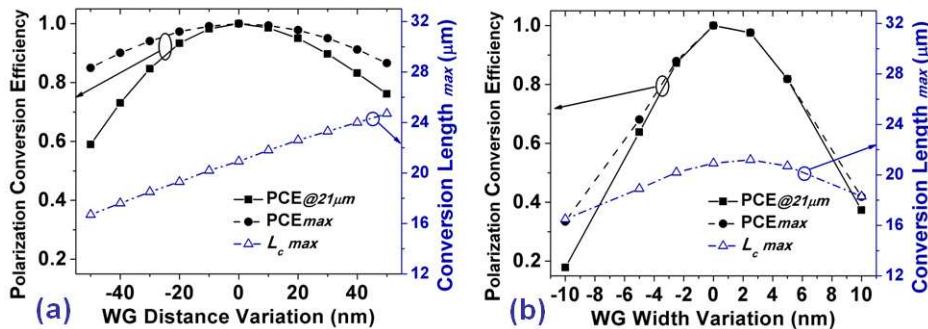


Fig. 7. (a) PCE@21 μ m, optimized PCE and its corresponding conversion length as a function of WG distance variation (ΔD). (b) PCE@21 μ m, optimized PCE and its corresponding conversion length as a function of WG width variation (ΔW).

5. Conclusion

We have proposed a polarization rotator using wave coupling through a multimode waveguide. A very short 21- μ m conversion length is achieved with a 17.22 dB extinction ratio. For PCE above 90%, the polarization rotator exhibits a 68-nm bandwidth around 1543 nm. For the nonideal fabrication, we can always choose a corresponding WG length and operating wavelength to enhance the PCE performance of the polarization rotator.

Acknowledgments

This work is sponsored by DARPA (under contract numbers N66001-08-1-2058) and HP Laboratories Innovation Research Awards.